On the Discrete-Input Continuous-Output Memoryless Channel Capacity of Layered ACO-OFDM

Xiaoyu Zhang, *Student Member, IEEE*, Sheng Chen, *Fellow, IEEE*, and Lajos Hanzo, *Fellow, IEEE*

(Invited Paper)

***Abstract*—Layered Asymmetrically Clipped Optical Orthogonal Frequency Division Multiplexing (LACO-OFDM) has been proposed for optical communications and has attracted much attention, thanks to its flexibility in terms of power vs. spectral efficiency. In this article, we propose algorithms for optimizing the Discrete-input Continuous-output Memoryless Channel (DCMC) capacity of LACO-OFDM. Then, an algorithm is proposed for maximizing the capacity for twin-layer LACO-OFDM by optimizing the power sharing between the layers. This is followed by the conception of a more general algorithm applicable to LACO-OFDM having an arbitrary number of layers. Numerical results are provided for quantifying the capacity improvement attained by the proposed algorithm. Moreover, an adaptive scheme is proposed for adjusting the number of layers to be used for maximizing the capacity at different SNRs.**

***Index Terms*—LACO-OFDM, capacity, optimization, power sharing, adaptive.**

I. Introduction

OPTICAL Wireless Communication (OWC) is expected to play a role as a potential component of next generation wireless systems, as a benefit of its low delay and low power consumption, as well as high integrity [1], [2]. Apart from these benefits, the substantial unlicensed visible light band spanning roughly from 400 to 800 THz band can be readily exploited by low-cost off-the-shelf transmitters, such as Light-Emitting Diodes (LEDs) [3]. Intensity Modulation combined with Direct Detection (IM/DD) has attracted much attention as a benefit of its low-cost components [4]. Following Armstrong's seminal contribution, the popularity of Orthogonal Frequency Division Multiplexing (OFDM) has grown in OWC, since its design has been well understood in the Radio Frequency (RF) industry [5]–[7]. While RF-OFDM produces complex-valued signals, the IM/DD can only handle pure real and non-negative values, which has led to several proposals for OWC-specific OFDM (O-OFDM) schemes [7].

Historically, Carruthers and Kahn exploited that OFDM symbols having Hermitian-symmetry in their Frequency Domain (FD) have real-valued Time Domain (TD) representations after Inverse Fast Fourier Transform (IFFT) based modulation, which leads to their proposal of Direct Current (DC) biased Optical OFDM (DCO-OFDM) [8]. Then, the resultant TD signal having negative and positive values is offset by a sufficiently high DC voltage for ensuring that the resultant signal only has negligible negative samples. These small negative samples are then clipped before intensity modulation. In 2006, the Asymmetrically Clipped Optical OFDM (ACO-OFDM) philosophy was proposed by Armstrong and Lowery for mitigating the high power consumption of the DC-offset and for reducing the clipping-induced distortion in DCO-OFDM [9]. In addition to the 50% throughput loss imposed by the Hermitian symmetry requirement, the ACO-OFDM scheme leaves all the even-indexed subcarriers blank in the FD for ensuring that clipping the negative contributions results in FD distortions falling onto the blank subcarriers. As an explicit benefit, the subcarriers loaded with information symbols are then free from distortion and in this way no information contamination occurs, but unfortunately this further halves the throughput. More explicitly, while ACO-OFDM avoids the high power consumption of DCO-OFDM, hence requiring a lower SNR, this is facilitated by transmitting only half the information within the same bandwidth [10]. This then leads to a power- vs. spectral- efficiency trade-off, when deciding which scheme to utilize. But naturally, the power saved by using blank subcarriers may be invested into the active subcarriers either for reducing their BER or for enhancing their throughput [11], [12].

Hence, several solutions have been conceived for striking a compromise between the power consumption and bandwidth efficiency [13]–[16]. Layered ACO-OFDM (LACO-OFDM) proposed by Wang *et al.* [15] is one of the recent breakthroughs. But a variety of other schemes, such as the Spectral and Energy Efficient OFDM (SEE-OFDM) scheme of [17], [18], the enhanced ACO-OFDM arrangement (eACO-OFDM [19]

Manuscript received January 14, 2020; revised April 9, 2020; accepted May 13, 2020. Date of publication May 21, 2020; date of current version September 15, 2020. The work of L. Hanzo was supported in part by the Engineering and Physical Sciences Research Council Projects EP/P034284/1, EP/P034284/1, and EP/P003990/1 (COALESCE) of the Royal Society's Global Challenges Research Fund Grant and in part by the European Research Council's Advanced Fellow Grant QuantCom. The data from the article can be obtained from the University of Southampton institutional repository: https://doi.org/10.5258/SOTON/D1380. *(Corresponding author: Lajos Hanzo.)*

The authors are with the School of Electronics and Computer Science, University of Southampton, Southampton SO17 1BJ, U.K. (e-mail: xz3u13@ecs.soton.ac.uk; sqc@ecs.soton.ac.uk; lh@ecs.soton.ac.uk).

Color versions of one or more of the figures in this article are available online at https://ieeexplore.ieee.org.

Digital Object Identifier 10.1109/JLT.2020.2996541

and EACO-OFDM [20]) as well as the enhanced U-OFDM (eU-OFDM) of [21], [22], have also relied on a similar philosophy. In simple tangible terms, LACO-OFDM strategically exploits the subcarriers left blank by ACO-OFDM and loads an additional ACO-OFDM signal onto them. The additional signal, termed as the *second* layer, has half the bandwidth of the original ACO-OFDM (referred to as the *first* layer), thus improving the overall bandwidth efficiency by 50%. After the superposition of the two layers, the resultant signal is known as a 2-layer (or twin-layer) LACO-OFDM signal. This operation can be repeated by exploiting the remaining blank subcarriers, loading the *third*, *fourth* and other layers. Naturally, transmitting more layers increases the overall power consumption. Therefore, LACO-OFDM beneficially improves the spectral efficiency of ACO-OFDM at the cost of reducing its power efficiency [23]–[25], striking a flexible trade-off.

Recent studies of the LACO-OFDM capacity [26]–[29], have been focused on the Continuous-input Continuous-output Memoryless Channel (CCMC) capacity, which is unbounded and as dictated by Shannon's ubiquitous capacity formula [30], subject to the unipolar IM/DD constraint. To expound a little further, Li *et al.* [26] studied the CCMC capacity of ACO-OFDM under both AWGN and fading channels. The CCMC capacity of LACO-OFDM was derived in [27] by Zhou and Zhang, who also compared it with other O-OFDM schemes. On the other hand, the Discrete-input Continuous-output Memoryless Channel (DCMC) capacity of LACO-OFDM requires more attention.

According to Shannon's formula, the CCMC capacity constitutes a loose upper bound of a system's throughput, because it is only dependent on the system's bandwidth and the channel SNR. This makes its calculation straightforward, but it relies on the idealized simplifying assumption that the transmitted signal is random Gaussian distributed. However, in reality we use discrete-time, discrete-amplitude modulated signals, which only become continuous-time, continuous-amplitude signals after baud-limiting filtering. By taking this into account, the DCMC capacity of a system provides a tighter upper bound of the achievable throughput of a system. More explicitly, the DCMC capacity takes into account the choice of the specific digital modulation schemes utilized for transmission. Therefore, the DCMC capacity is more widely used for evaluating the throughput of a system, especially upon considering the benefits of channel coding in the quest for near-capacity operation. However, the calculation of the DCMC capacity is not as straightforward as that of the CCMC capacity, which is tackled in this paper. Naturally, the DCMC capacity is a more realistic bound, since practical discrete modulation schemes are considered. It was revealed in [31] that modulation schemes whose modulation-order is excessively high may not be suitable for O-OFDM, given their vulnerability to clipping distortion.

Against this background, we focus our attention on maximizing the total DCMC capacity of a LACO-OFDM system. Explicitly, our contributions may be summarized as follows:

- We derive the DCMC capacity of a LACO-OFDM system as a function of the Signal-to-Noise Ratio (SNR) and the number of layers in the system, as well as the power sharing amongst the layers. In this paper, the DCMC capacity is hereafter referred to as "channel capacity" or simply "capacity".
- We provide an algorithm for determining the optimum power-sharing strategy for twin-layer LACO-OFDM at a given SNR, followed by our generalized algorithm.
- Finally, we compare the optimized capacities of LACO-OFDM systems relying on different number of layers, which leads to an adaptive scheme using the optimum number of layers for maximizing the capacity at a given SNR.

A. Paper Structure

This paper is organized as follows. In Section II, the architecture of the LACO-OFDM transceiver is discussed, followed by our DCMC capacity expression derived in Section III. Section IV focuses on the optimization of a twin-layer LACO-OFDM system's capacity, which is then extended to a system having three or more layers in Section V. The algorithm proposed is further evaluated in Section VI. Finally, Section VII concludes this paper.

B. Nomenclature

We use C, P and Γ to represent the capacity, power and SNR, respectively, as defined formally in due course. Their subscript represents a standalone layer of the LACO-OFDM scheme, while "RF," "ACO" and "LACO" refer to the overall multi-layer scheme. For example, P_{LACO} represents the total power of the LACO-OFDM system, while P_2 represents the power of the 2nd layer in a LACO-OFDM system.

Furthermore, $\frac{\partial f}{\partial x}$ is the partial derivative of the function f with respect to x, while $\frac{\partial f}{\partial x}|_{x_0}$, $\frac{\partial f}{\partial x}|_{g(x_0)}$ is the value of the derivative at the points of $x = x_0$ and $x = g(x_0)$, respectively. In addition, $\frac{\partial h}{\partial x}|_{(x_0,y_0)}$ evaluates the partial derivative of h with respect to x at the point (x_0, y_0).

II. System Model

We commence by introducing the optical channel model we adopted, followed by the basic structure of an ACO-OFDM system, before expounding further on more sophisticated LACO-OFDM systems. In addition, the schematic of LACO-OFDM to be introduced in this paper also features FEC channel coding modules proposed in [24].[1] for for exploiting its low inter-layer interference (ILI).

A. Channel Model

Based on pioneering work of Wang *et al.* on LACO-OFDM [15], we consider the following indoor Visible Light Communications (VLC) downlink scenario. In our assumption, a single LED acts as the transmitter that serves a user within the room. As it has been shown in our previous work [23], the LACO-OFDM scheme is capable of drastically reducing the signal's PAPR, hence we may assume that the LED operates

[1]This coded LACO-OFDM is termed as multi-class coded LACO-OFDM in [24].

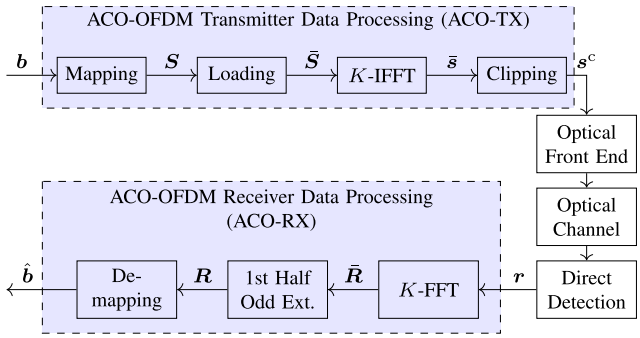

Fig. 1. Schematic of an ACO-OFDM transmitter.

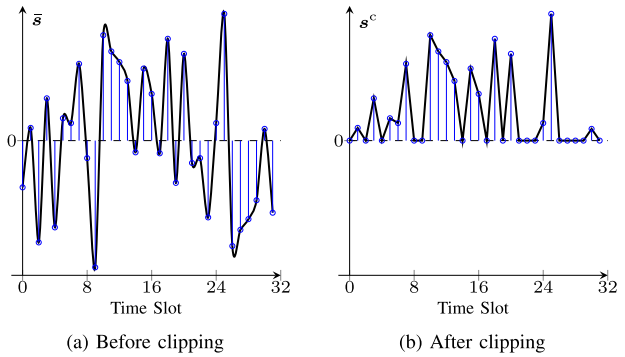

(a) Before clipping (b) After clipping

Fig. 2. Examples of an ACO-OFDM TD signal for $K = 32$ subcarriers in the FD.

within its linear range, where no upper clipping occurs. An additive white Gaussian noise (AWGN) channel is considered in this paper, which is an appropriate assumption for line-of-sight VLC scenarios, as it has been configured for IM/DD performance analysis in [31]–[33].

B. ACO-OFDM

Fig. 1 shows the schematic of an ACO-OFDM system, where the shaded area at the top represents the transmitter (ACO-TX), and the one at the bottom the receiver (ACO-RX). An example of the TD ACO-OFDM signal is also presented in Fig. 2.

The input bit stream $\boldsymbol{b}$ of the ACO-TX is firstly mapped [2] to the discrete symbols of a given Quadrature Amplitude Modulation (QAM) or Phase Shift Keying (PSK) constellation pattern. The symbols $\boldsymbol{S} = \{S[0], S[1], \ldots, S[k], \ldots\}$ are then loaded[3] to the stream $\bar{\boldsymbol{S}}$ under the ACO-OFDM loading rule of (1), where the ACO-OFDM scheme is capable of conveying $K/4$ symbols mapped to K subcarriers, with $S^*[k]$ being the conjugate of symbol $S[k]$.

$$\bar{S}[u] = \begin{cases} S[k], & u = 2\,k + 1, \\ S^*[k], & u = K - (2\,k + 1), \\ 0, & \text{otherwise.} \end{cases} \quad \begin{array}{l} 0 \le u \le \frac{K}{4}, \\ 0 \le k \ \le K, \end{array} \tag{1}$$

[2]To avoid confusion, in this paper, we refer to bit-to-symbol "mapping" when we discuss the action of the "Mapping" block of Fig. 1 generating the stream $\boldsymbol{S}$ from $\boldsymbol{b}$. By contrast, the action of the "Loading" block of Fig. 1 is termed as "loading," which creates the symbol stream $\bar{\boldsymbol{S}}$ from $\boldsymbol{S}$, according to the ACO-OFDM rules.

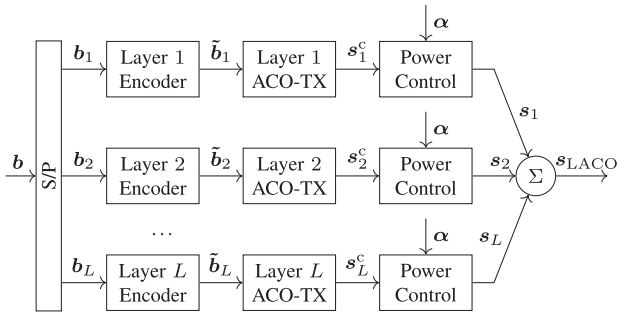

Fig. 3. Schematic diagram of a LACO-OFDM transmitter using FEC encoding, where each "ACO-TX" block is similar, but not identical to the architecture of Fig. 1.

The resultant signal is processed by a K-point IFFT, which transforms it to its TD counterpart $\bar{\boldsymbol{s}} = \{\bar{s}[0], \bar{s}[1], \ldots\}$. The mapping rule (1) enforces the Hermitian symmetry in $\bar{\boldsymbol{S}}$, which ensures that the TD signal $\bar{\boldsymbol{s}}$ is purely real-valued, as the example shown in Fig. 2(a). Moreover, (1) maps a null symbol to all the even-indexed subcarrier, which results in further symmetry formulated $\bar{\boldsymbol{s}}$ as

$$\bar{s}[k] = -\bar{s}[K - k], \tag{2}$$

which can also be observed from Fig. 2(b). Hence, despite clipping all negative samples in $\bar{\boldsymbol{s}}$, all the information can be losslessly recovered from the resultant signal $\boldsymbol{s}^{\mathrm{c}}$, as shown in Fig. 2(b). The clipped signal $\boldsymbol{s}^{\mathrm{c}}$ is unipolar, thus it can be forwarded to the optical front end of Fig. 1.

The received signal of Fig. 1 is then converted back to the electric TD by the direct detection block of Fig. 1, yielding the signal $\boldsymbol{r}$, before passing it to the ACO-RX block. The unipolar signal $\boldsymbol{r}$ is firstly transformed back to the FD signal $\bar{\boldsymbol{R}}$ of length K by the K-point FFT. Again, the "lossless clipping" operation imposed by the ACO-TX block of Fig. 1 actually results in clipping distortions that are accommodated by the even-indexed subcarriers, *i.e.* those marked in (1) as "otherwise". Therefore, the desired symbols can be readily extracted from the first $K/4$ odd-indexed subcarriers of $\bar{\boldsymbol{R}}$ ($\bar{R}[1], \bar{R}[3], \ldots, \bar{R}[K/2 - 1]$) to form $\boldsymbol{R}$ of Fig. 1. Following symbol-to-bit constellation demapping, the receiver obtains the information bits $\hat{\boldsymbol{b}}$.

C. LACO-OFDM Transmitter Using FEC Encoding

Fig. 3 shows the detailed layer-based schematic of a LACO-OFDM transmitter using FEC encoding. A group of examples of the TD representations of a 3-layer LACO-OFDM signal and its constituent layer signals (before and after clipping) is also given in Fig. 4.

In LACO-OFDM, the original bit stream is split into L layers as $\{\boldsymbol{b}_1, \ldots, \boldsymbol{b}_L\}$. Forward Error Correction (FEC) channel encoders are employed for each individual layer's bit streams, producing the channel-encoded stream $\{\tilde{\boldsymbol{b}}_1, \ldots, \tilde{\boldsymbol{b}}_L\}$, each having its own ACO-TX block similar to, but not identical to, that of Fig. 1. Explicitly, the following modifications have to be carried out for ensuring that the symbols mapped to higher layers (*i.e.* those having a higher layer index l) always fall on the subcarriers left blank by the lower layers. Explicitly, the loading rule for the

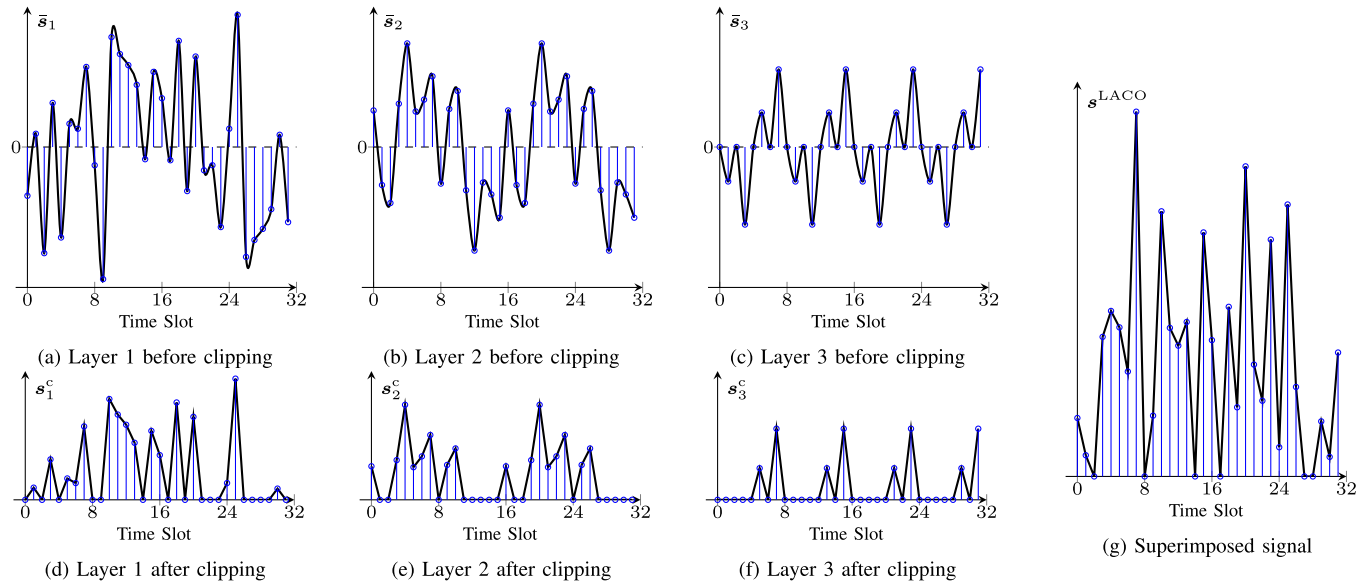

Fig. 4. Example of the TD representations of a LACO-OFDM signal and its 3 constituent layers for $K = 32$ subcarriers in the FD.

lth layer is now:

$$\bar{S}_l[u] = \begin{cases} S_l[k], & u = 2^l k + 2^{l-1}, \\ S_l^*[k], & u = K - (2^l k + 2^{l-1}), \\ 0, & \text{otherwise}, \end{cases}$$

$$1 \le l \le L,\ 0 \le u \le \frac{K}{2^{l+1}} \text{ for } S_l[k], 0 \le k \le K, \qquad (3)$$

where $S_l[k]$ is the kth symbol for the lth layer.

Hence, the lth layer is capable of accommodating $K/2^{l+1}$ symbols, *i.e.* the signal $\bar{\boldsymbol{S}}_l$ should have $K/2^{l+1}$ non-zero subcarriers. Therefore, LACO-OFDM having L layers is capable of conveying a total of $[(K/2) \times (1 - 1/2^L)]$ symbols, nearly doubling the normalized throughput of the ACO-OFDM scheme. The signals loaded onto each layer of Fig. 3 are then independently subjected to K-point IFFT, whose output should obey (2), which can have all its negative samples clipped in order to form the unipolar signals $\boldsymbol{s}_l$. Meanwhile, observe from the examples given in Fig. 4, where Figs. 4(a–c) are the unclipped signals and Figs. 4(d–f) are the clipping signals, that repetitions occur in layer 2 and 3 signals, because of their halved and quartered number of modulated subcarriers in the FD, compared to layer 1, respectively.

Observe in Fig. 3 that a power control module is employed after clipping for ensuring that each layer has the most appropriate power share. A set of power sharing factors $\boldsymbol{\alpha} = \{\alpha_1, \alpha_2, \ldots \alpha_{L-1}\}$ is used by these power controllers for ensuring that the signal $\boldsymbol{s}_l$ has an electric power of P_l. This process will be further discussed in Secs. IV and V.

Finally, the signals having the optimal power are superimposed for constructing the TD signal $\boldsymbol{s}_{\text{LACO}}$, which completes the LACO-OFDM transmitter's signal processing actions seen in Fig. 6.

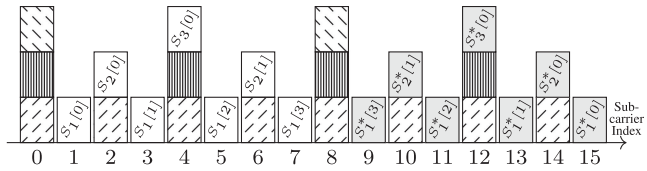

Fig. 5. FD representation of a 3-layer LACO-OFDM signal having 16 subcarriers [23]. The "North-East" hatching, vertical hatching and "North-West" hatching represent the clipping distortions of the 1st, 2nd and 3 rd layer, respectively.

D. Frequency Domain Representations of LACO-OFDM

To elaborate further on the operation of LACO-OFDM, the FD representation of a 3-layer LACO-OFDM signal is portrayed in Fig. 5.

According to (3), the symbols $S_1[0]$, $S_1[1]$, $S_1[2]$ and $S_1[3]$ assigned to the first layer occupy subcarriers 1, 3, 5, and 7, while their respective conjugates are loaded onto subcarriers 15, 13, 11 and 9. After clipping the negative part of the TD signal, the distortions generated will only contaminate the even-indexed subcarriers, *i.e.* $k = 0, 2, \ldots, 14$, thanks to the property of "lossless clipping" inherited from ACO-OFDM. The 1st layer's distortions are represented by the "North-East" hatching in Fig. 5.

Similarly, for the 2nd layer, the symbols are loaded onto the subcarriers at $k = 2, 6$, while their conjugates onto $k = 14, 10$ and their clipping distortions contaminate the subcarriers $k = 0, 4, 8, 12$ marked by vertical hatching. When $k = 16$, the 3 rd layer may only have 1 symbol, which is located at subcarrier $k = 4$ and has its conjugate at subcarrier $k = 12$, while its clipping distortions are represented by the "North-West" hatching blocks at subcarriers $k = 0$ and $k = 8$.

Therefore, in LACO-OFDM, a subcarrier-symbol can only be placed together with distortions produced from its lower layers,

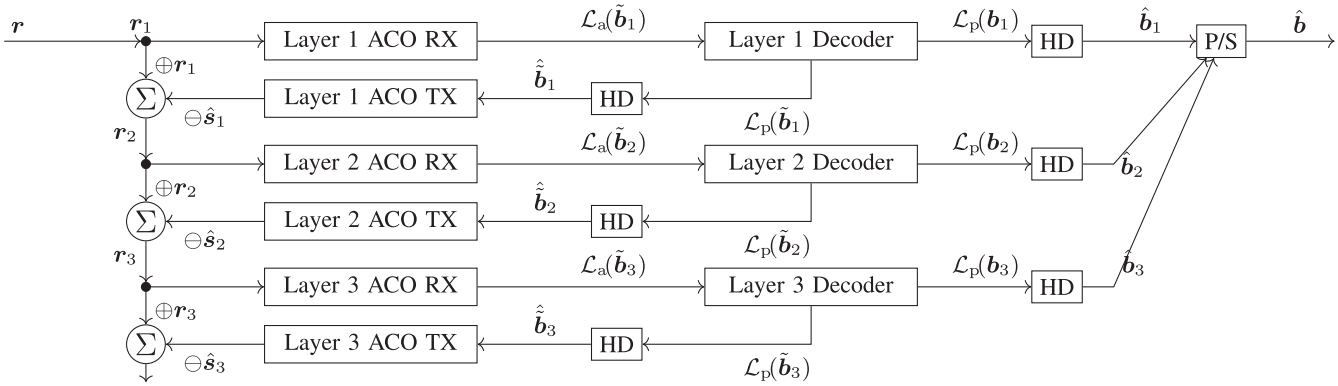

Fig. 6. Schematic diagram of a LACO-OFDM receiver using FEC decoding, where the "HD" blocks represent hard decision operation. The definitions of all the appeared variables are summarized in Tab. I.

but it remains orthogonal to all other subcarrier-symbols of the same layer. Moreover, the symbols of the 1st layer are entirely free from clipping distortion, hence they can be directly detected without resorting to interference-cancellation. By contrast, the upper layers have to be decontaminated from the distortion products imposed by the lower layers. But fortunately, this can be readily achieved by an iterative clean-up operation commencing with the uncontaminated 1st layer.

E. LACO-OFDM Receiver Using FEC Decoding

Based on the discussions of Section II-D, let us now present the receiver design of LACO-OFDM using FEC decoding, which is shown in Fig. 6.

Based on classic direct detection, the received optical signal is first converted into its electric domain representation by a photo detector, and then from the TD to its FD representation by the K_l-point FFT, like for the ACO-OFDM signal of Fig. 1. The subcarrier detection of a LACO-OFDM signal at the receiver commences from the uncontaminated first layer, whose symbols are completely free from the interference produced by the clipping distortion. Hence, they can be directly extracted. A soft-output QAM demapper is employed to calculate the *a priori* Log-Likelihood Ratio (LLR) of the encoded bits $\mathcal{L}_{\rm a}(\tilde{\boldsymbol{b}}_1)$ from the extracted symbol stream $\hat{\boldsymbol{S}}_1$. This information will be forwarded to a channel decoder having the corresponding FEC code paired with the FEC encoder of Fig. 3, which provides the *a posteriori* LLR of the uncoded bit stream $\mathcal{L}_{\rm p}(\boldsymbol{b}_1)$. Following hard-decision (HD), the detected bit stream $\hat{\boldsymbol{b}}_1$ of layer 1 is obtained. The soft-output demapper also generates the *a posteriori* LLR $\mathcal{L}_{\rm p}(\tilde{\boldsymbol{b}}_1)$ of the coded bit stream for a better estimation of $\hat{\boldsymbol{b}}_1$, which will then be re-modulated to reconstruct the layer's unipolar signal $\hat{\boldsymbol{s}}_1$ at the receiver by going through the entire modulation process of mapping, loading, IFFT, clipping and power sharing, as seen in Fig. 6. In this way, the TD-clipping-induced FD distortions caused by the 1st layer can be reproduced at the receiver, which can then be subtracted from the received signal. Viewing this process in Fig. 5, it wipes out all interference products at the "bottom level" of that tripple-level structure.

Still referring to Fig. 5, it becomes clear that the symbols on the 2nd layer are now free from the TD-clipping-induced FD interference as well. The detection process of the 1st layer can then be repeated for the 2nd layer, reproducing the locally reconstructed 2nd layer information bits and wiping out the interference, as seen in Fig. 6. This is followed by the same detection process for the 3 rd layer, and if applicable to the 4th layer and so on.

Finally, the bits output by each layer are combined into a single bit stream and form the final output stream.

III. DCMC Capacity of LACO-OFDM

A. DCMC Capacity of an RF-OFDM System

Let us define the channel SNR Γ as the channel energy per symbol (E_s) to noise power spectral density (N_0) ratio, namely as $\Gamma = E_s^{(\rm RF)}/N_0$ for an RF system, where the superscript on E_s is for indicating the modulation technique of the signal. The channel capacity of an M-QAM scheme is [34], [35]

$$\begin{aligned} C_{\rm RF}(\Gamma) &= (\text{Sink Entropy}) - (\text{Noise Entropy}) \\ &= \underbrace{-\int_{-\infty}^{\infty} p(R)\log_2\left[p(R)\right]\,{\rm d}R}_{\rm (a)} \underbrace{-\log_2\left(\frac{\pi e}{\Gamma}\right)}_{\rm (b)}, \end{aligned} \quad (4)$$

where the definitions of each part are given below:

- Part (b) in (4) represents the entropy of the noise, which is complex-valued having a variance of N_0.
- In part (a) of (4), the integration should take place across the entire complex-valued plane, if high order modulation ($M > 2$) is applied, where the probability $p(R[n])$ of the received symbols is given by

$$\begin{aligned} p(R[n]) &= \frac{1}{M}\sum_{m=1}^{M} p(R[n]|\mathcal{S}^{(m)}) \\ &= \frac{1}{M}\sum_{m=1}^{M}\left[\frac{\Gamma}{\pi}\cdot\exp\left(-\Gamma\cdot\left|R[n]-\mathcal{S}^{(m)}\right|^2\right)\right] \\ &= \frac{\Gamma}{\pi M}\sum_{m=1}^{M}\exp\left(-\Gamma\cdot\left|R[n]-\mathcal{S}^{(m)}\right|^2\right), \end{aligned} \quad (5)$$

where $\mathcal{S}^{(m)}$ is the mth points in the MQAM constellation $\mathcal{S}$ having a unity average power, and $p(R[n]|\mathcal{S}^{(m)})$ is the complex-valued Gaussian distribution PDF with a mean of $\mathcal{S}^{(m)}$ and variance of $1/\Gamma$.

Unfortunately, part (a) of (4) cannot be analytically evaluated, due to the summation within the logarithm shown in (5). However, Monte-Carlo method can be used for approximating it by generating a sufficiently high number of received symbol realizations ($\boldsymbol{R} = R[1], R[2], \ldots, R[n], \ldots$), yielding

$$(\mathrm{a}) = \mathbb{E}\left[-\log_2(p(R))\right] \approx -\frac{1}{N}\sum_{n=1}^{N}\log_2\left[p(R[n])\right], \tag{6}$$

where $\mathbb{E}[\cdot]$ is the statistical expectation, and the approximation converges as $N \to \infty$. Hence, (4) can be simplified as:

$$\begin{aligned} C_{\mathrm{RF}}(\Gamma) &\approx -\log_2\left(\frac{\pi e}{\Gamma}\right) \\ &- \frac{1}{N}\sum_{n=1}^{N}\log_2\left[\frac{\Gamma}{\pi M}\sum_{m=1}^{M}\exp\left(-\Gamma\cdot\left|R[n]-\mathcal{S}^{(m)}\right|^2\right)\right] \\ &= -\frac{1}{N}\sum_{n=1}^{N}\log_2\left[\frac{e}{M}\sum_{m=1}^{M}\exp\left(-\Gamma\cdot\left|R[n]-\mathcal{S}^{(m)}\right|^2\right)\right], \end{aligned} \tag{7}$$

where the "$\approx$" sign can be replaced by "$=$" as $N \to \infty$.

Moreover, the derivative of C_{RF} with respect to Γ indicates the sensitivity of channel capacity to SNR changes, expressed as

$$\frac{\partial C_{\mathrm{RF}}}{\partial \Gamma} = \frac{\sum_{n=1}^{N}\left[\frac{\sum_{m=1}^{M}\left|R[n]-\mathcal{S}^{(m)}\right|^2\exp\left(-\Gamma\cdot\left|R[n]-\mathcal{S}^{(m)}\right|^2\right)}{\ln 2\cdot\sum_{m=1}^{M}\exp\left(-\Gamma\cdot\left|R[n]-\mathcal{S}^{(m)}\right|^2\right)}\right]}{N}. \tag{8}$$

B. DCMC Capacity of an ACO-OFDM System

Recall from Section II that in ACO-OFDM only $K/4$ symbols can be conveyed by a total of K subcarriers. Therefore, the channel capacity contribution can be divided into two parts:

- The $3K/4$ subcarriers loaded either with the conjugate of the transmitted symbols or with the FD-product of the TD clipping distortion, whose capacity-contribution is 0, because they provide no new information, and
- The $K/4$ subcarriers loaded with the desired transmitted symbols.

The $K/4$ FD subcarriers in the second part may be viewed as isolated RF carriers, where (4) can be applied. Therefore, the capacity of an ACO-OFDM system is given by

$$C_{\mathrm{ACO}}(\Gamma) = \frac{K/4}{K}C_{\mathrm{RF}}(\Gamma) + \frac{3K/4}{K}\cdot 0 = \frac{1}{4}C_{\mathrm{RF}}(\Gamma), \tag{9}$$

where the proportionality coefficient $1/4$ represents the reduced bandwidth efficiency.

Since the total signal power P_{ACO} is equally spread across the $K/4$ transmitted subcarrier symbols (25%), the $K/4$ conjugate symbols (25%) and the $K/2$ distortion symbols (50%), we have

$$\Gamma_{\mathrm{ACO}} = \frac{E_s^{(\mathrm{ACO})}}{\frac{1}{2}N_0} = \frac{\frac{1}{4}P_{\mathrm{ACO}}}{\frac{K/4}{K}\frac{1}{2}N_0} = \frac{P_{\mathrm{ACO}}}{\frac{1}{2}N_0}, \tag{10}$$

where the factor $\frac{1}{2}$ in the denominator is because the imaginary part of the complex-valued TD noise has no effect on the performance.

C. Power Relationships in LACO-OFDM

Without loss of generality, we denote the electric signal power of the lth layer in LACO-OFDM as P_l. The TD signal obeys a one-sided truncated Gaussian distribution [23] with the PDF given by

$$\mathrm{PDF}(x) = \frac{1}{2}\delta(x) + \frac{1}{\sqrt{2\pi}\sigma}\exp\left[-\frac{x^2}{2\sigma^2}\right]u(x), \tag{11}$$

where $\delta(\cdot)$ and $u(\cdot)$ are the Dirac delta function and Heaviside step function, respectively, while σ^2 is the variance of the signal before truncation. The power of a layer is then represented as

$$P_l = \int_{-\infty}^{\infty} x^2\cdot\mathrm{PDF}(x)\mathrm{d}x = \frac{1}{2}\sigma^2, \tag{12}$$

because the truncation cuts half of the power. Furthermore, the mean and variance of a layer's signal can be expressed using P_l as

$$\begin{aligned} \mathbb{E}[s_l] &= \int_{-\infty}^{\infty} x\cdot\mathrm{PDF}(x)\mathrm{d}x = \frac{\sigma}{\sqrt{2\pi}} = \sqrt{\frac{P_l}{\pi}}, \\ \mathbb{D}[s_l] &= \int_{-\infty}^{\infty}(x-\mathbb{E}[s_l])^2\cdot\mathrm{PDF}(x)\mathrm{d}x \\ &= \frac{\pi-1}{2\pi}\sigma^2 = \left(1-\frac{1}{\pi}\right)P_l. \end{aligned} \tag{13}$$

The overall electric signal power P_{LACO} could be expressed by its mean and variance as

$$P_{\mathrm{LACO}} = \mathbb{D}[s] + \left(\mathbb{E}[s]\right)^2, \tag{14}$$

where both the mean and variance are the sum of their L constituent layers, given by:

$$\begin{aligned} P_{\mathrm{LACO}} &= \left(\sum_{l=1}^{L}\mathbb{D}[s_l]\right) + \left(\sum_{l=1}^{L}\mathbb{E}[s_l]\right)^2 \\ &= \left[\sum_{l=1}^{L}\left(1-\frac{1}{\pi}\right)P_l\right] + \left(\sum_{l=1}^{L}\sqrt{\frac{P_l}{\pi}}\right)^2 \\ &= \left(1-\frac{1}{\pi}\right)\sum_{l=1}^{L}P_l + \frac{1}{\pi}\left(\sum_{i=1}^{L}\sum_{j=1}^{L}\sqrt{P_i}\sqrt{P_j}\right) \\ &= \sum_{l=1}^{L}P_l + \frac{2}{\pi}\sum_{i\neq j}\sqrt{P_iP_j}. \end{aligned} \tag{15}$$

D. DCMC Capacity of a LACO-OFDM System

Table II shows the composition of each layer of a LACO-OFDM signal. On the lth layer of a LACO-OFDM scheme, only $\frac{K}{2^{l+1}}$ information-earning symbols can be transmitted, complemented by $\frac{K}{2^{l+1}}$ subcarriers for themselves, and another $\frac{K}{2^{l+1}}$ subcarriers for their conjugates, as well as by the $\frac{K}{2^l}$ additional subcarriers occupied by the FD-products of the TD clipping

TABLE I
SUMMARY OF THE DEFINITIONS OF VARIABLES USED IN THE LACO-OFDM RECEIVER USING FEC DECODING OF FIG. 6

Notation	Definition
$\boldsymbol{r}$	Originally received signal
$\boldsymbol{r}_l$	Received signal for detecting layer l, where the ILIs of all its previous layers have been removed
$\mathcal{L}_{\rm a}(\tilde{\boldsymbol{b}}_l)$	The *a priori* LLR of the coded bit stream $\tilde{\boldsymbol{b}}_l$, produced by the QAM demapper
$\mathcal{L}_{\rm p}(\tilde{\boldsymbol{b}}_l)$	The *a posteriori* LLR of the coded bit stream $\tilde{\boldsymbol{b}}_l$ for ILI cancellation, produced by the FEC decoder
$\hat{\tilde{\boldsymbol{b}}}_l$	Hard estimate of the transmitted coded bit stream $\tilde{\boldsymbol{b}}_l$, produced by HD
$\hat{\boldsymbol{s}}_l$	Receiver's estimate of the clipped layer signal $\boldsymbol{s}_l$ to be cancelled from $\boldsymbol{r}_l$, before progressing to the detection of the next layer
$\mathcal{L}_{\rm p}(\boldsymbol{b}_l)$	The *a posteriori* LLR of the uncoded bit stream $\boldsymbol{b}_l$ for layer detection, produced by the FEC decoder
$\hat{\boldsymbol{b}}_l$	Hard estimate of the transmitted uncoded bit stream $\boldsymbol{b}_l$, produced by HD
$\hat{\boldsymbol{b}}$	Consolidated detected bit stream

TABLE II
COMPOSITION OF AN LACO-OFDM SIGNAL SHOWING THE NUMBER OF SUBCARRIERS ($\mathcal{N}$) AND AVERAGE SYMBOL POWER ($\mathcal{P}$) OF THE FOUR PARTS OF EACH LAYER: DESIRED TRANSMITTED SYMBOLS (TX), CONJUGATE SYMBOLS (CONJ.), CLIPPING DISTORTIONS OF THE CURRENT LAYER (DIST.) AND IDLE SUBCARRIERS AFTER CLIPPING (IDLE)

Layer Index	Layer Power	TX or Conj.		Dist.		Idle	
		$\mathcal{N}$	$\mathcal{P}$	$\mathcal{N}$	$\mathcal{P}$	$\mathcal{N}$	$\mathcal{P}$
1	P_1	$\frac{1}{4}K$	P_1	$\frac{1}{2}K$	P_1	0	0
2	P_2	$\frac{1}{8}K$	$2P_2$	$\frac{1}{4}K$	$2P_2$	$\frac{1}{2}K$	0
3	P_3	$\frac{1}{16}K$	$4P_3$	$\frac{1}{8}K$	$4P_3$	$\frac{3}{4}K$	0
				...			
l	P_l	$\frac{K}{2^{l+1}}$	$2^{l-1}P_l$	$\frac{K}{2^l}$	$2^{l-1}P_l$	$\frac{2^{l-1}-1}{2^{l-1}}K$	0
				...			

distortion. The power allocated to the lth layer shall be (statistically) equally shared among these $\frac{K}{2^{l-1}}$ subcarriers, which results in $2^{l-1}P_l$ for each subcarrier. The remaining $(1-\frac{1}{2^{l-1}})K$ subcarriers are left empty, having zero power.

Given a sufficiently high SNR, the receiver can be expected to fully cancel out the TD-clipping distortions with the help of forward error correction codes (FEC) [24]. When detecting the lth layer at the receiver, its SNR Γ_l would be calculated using the power of the subcarriers loaded with the symbols, yielding

$$\Gamma_l = \frac{2^{l-1}P_l}{N_0/2}. \tag{16}$$

For LACO-OFDM, its first layer signal is constituted by an ACO-OFDM signal. As a result, the capacity contribution of LACO-OFDM from its first layer is:

$$C_1(\Gamma_1) = C_{\rm ACO}(\Gamma_1) = \frac{1}{4}C_{\rm RF}(\Gamma_1). \tag{17}$$

Similarly, for the second and higher layer signals, their transmission rate contribution can be written as

$$C_l(\Gamma_l) = \frac{1}{2^{l-1}}C_{\rm ACO}(\Gamma_1) = \frac{1}{2^{l+1}}C_{\rm RF}(\Gamma_l). \tag{18}$$

Therefore, the overall capacity of a LACO-OFDM system having a total of L layers can be written as

$$C_{\rm LACO} = \sum_{l=1}^{L} C_l(\Gamma_l) = \sum_{l=1}^{L} \frac{1}{2^{l+1}}C_{\rm RF}(\Gamma_l). \tag{19}$$

Explicitly, $C_{\rm LACO}$ is a function of the individual SNR of each layer $(\Gamma_1, \Gamma_2, \ldots, \Gamma_L)$, which is in turn a function of the power allocated to each layer $(P_1, P_2, \ldots, P_L)$, subject to the constraint

$$0 \le P_l \le P_{\rm LACO}, \forall l,$$
$$\text{and } (15). \tag{20}$$

IV. CAPACITY MAXIMIZATION FOR TWIN-LAYER LACO-OFDM

In this section, the total power and capacity of a twin-layer LACO-OFDM system, *i.e.* $P^{(2)}_{\rm LACO}$ and $C^{(2)}_{\rm LACO}$, represent $P_{\rm LACO}$ and $C_{\rm LACO}$, respectively.

A. Capacity of Twin-Layer LACO-OFDM

Let us consider a LACO-OFDM system consisting of 2 layers only and define the power sharing factor α $(0 \le \alpha \le 1)$ as the specific fraction of the total power belonging to layer 1. Naturally, the second layer has then $(1-\alpha)$ portion of the power, *i.e.* we have

$$\frac{P_1}{P_2} = \frac{\alpha}{1-\alpha}. \tag{21}$$

Substituting this into (15), we arrive at

$$\begin{aligned} P_{\rm LACO} &= P_1 + P_2 + \frac{2}{\pi}\sqrt{P_1 P_2} \\ &= P_1 + \frac{1-\alpha}{\alpha}P_1 + \frac{2}{\pi}\sqrt{P_1 \cdot \frac{1-\alpha}{\alpha}P_1} \\ &= P_1\left(\frac{1}{\alpha} + \frac{2}{\pi}\sqrt{\frac{1-\alpha}{\alpha}}\right). \end{aligned} \tag{22}$$

Therefore, P_1 can be represented as

$$P_1 = \frac{\alpha \cdot P_{\rm LACO}}{1 + \frac{2}{\pi}\sqrt{\alpha(1-\alpha)}}. \tag{23}$$

Similarly,

$$P_2 = \frac{(1-\alpha) \cdot P_{\rm LACO}}{1 + \frac{2}{\pi}\sqrt{\alpha(1-\alpha)}}. \tag{24}$$

For a given power constraint $P_{\rm LACO}$ and noise power N_0, the overall channel SNR of LACO-OFDM is defined as $\Gamma_{\rm LACO} = P_{\rm LACO}/(N_0/2)$. Using (16), the corresponding SNR of each of the two layers becomes

$$\Gamma_1 = \frac{P_1}{N_0/2} = \frac{\alpha \cdot \Gamma_{\rm LACO}}{1 + \frac{2}{\pi}\sqrt{\alpha(1-\alpha)}}, \tag{25a}$$

$$\text{and } \Gamma_2 = \frac{2P_2}{N_0/2} = \frac{2(1-\alpha)\cdot\Gamma_{\mathrm{LACO}}}{1+\frac{2}{\pi}\sqrt{\alpha(1-\alpha)}}. \tag{25b}$$

Note that the layer SNRs defined in (25) can be treated as a function of both the overall SNR Γ_{LACO} and the power sharing ratio α.

In this way, the overall capacity of this twin-layer LACO-OFDM system can be written according to (19) as

$$C_{\mathrm{LACO}} = C_1(\Gamma_1) + C_2(\Gamma_2) = \frac{C_{\mathrm{RF}}(\Gamma_1)}{4} + \frac{C_{\mathrm{RF}}(\Gamma_2)}{8}. \tag{26}$$

The chain rule of functions indicates that C_{LACO} shall also be a function of Γ_{LACO} and α. Therefore, the maximum throughput at a given SNR Γ can be determined by solving the following problem:

$$\begin{aligned} \max_{\alpha} \quad & C_{\mathrm{LACO}}(\Gamma_{\mathrm{LACO}}, \alpha) \\ \text{s.t.} \quad & 0 \le \alpha \le 1 \\ & \text{and } (22). \end{aligned} \tag{27}$$

B. Characteristics of C_{LACO}

1) Existence of Maxima: For a given Γ, C_{LACO} is non-negative by definition, having a lower bound of zero. On the other hand, the DCMC capacity is upper bounded by the general CCMC capacity [6] of

$$0 \le C_{\mathrm{LACO}}(\Gamma, \alpha) \le \log_2(1+\Gamma), \forall \alpha. \tag{28}$$

Since C_{LACO} is formed of elementary functions, it is also continuous within $\alpha \in [0,1]$. According to the extreme value theorem [36], at least one maximum must be attained by C_{LACO} for any given Γ within the interval $\alpha \in [0,1]$.

2) Monotonicity of SNRs: If we take the partial derivative of C_{LACO} in (26) with respect to α, we have

$$\begin{aligned} \frac{\partial C_{\mathrm{LACO}}}{\partial \alpha} &= \frac{\partial}{\partial \alpha}\frac{C_{\mathrm{RF}}(\Gamma_1)}{4} + \frac{\partial}{\partial \alpha}\frac{C_{\mathrm{RF}}(\Gamma_2)}{8} \\ &= \underbrace{\frac{1}{4}\underbrace{\frac{\partial C_{\mathrm{RF}}}{\partial \Gamma_1}}_{(\mathrm{c1})}\underbrace{\frac{\partial \Gamma_1}{\partial \alpha}}_{(\mathrm{c2})}}_{(\mathrm{c})} + \underbrace{\frac{1}{8}\underbrace{\frac{\partial C_{\mathrm{RF}}}{\partial \Gamma_2}}_{(\mathrm{d1})}\underbrace{\frac{\partial \Gamma_2}{\partial \alpha}}_{(\mathrm{d1})}}_{(\mathrm{d})}. \end{aligned} \tag{29}$$

Since the channel capacity is always monotonically non-decreasing vs. the SNR [6], we have

$$\frac{\partial C_{\mathrm{RF}}}{\partial \Gamma_1} \ge 0, \text{ and } \frac{\partial C_{\mathrm{RF}}}{\partial \Gamma_2} \ge 0. \tag{30}$$

Using (25), the partial derivative of Γ_1 with respect to α is

$$\begin{aligned} \frac{\partial \Gamma_1}{\partial \alpha} &= \frac{\partial}{\partial \alpha}\left(\frac{\alpha\cdot\Gamma_{\mathrm{LACO}}}{1+\frac{2}{\pi}\sqrt{\alpha(1-\alpha)}}\right) \\ &= \frac{\pi\left(\alpha+\pi\sqrt{(1-\alpha)\alpha}\right)\Gamma_{\mathrm{LACO}}}{\sqrt{(1-\alpha)\alpha}\left(2\sqrt{(1-\alpha)\alpha}+\pi\right)^2}, \end{aligned} \tag{31}$$

where C_{LACO} is locally treated as a positive constant. Symbolic analysis of (31) in Section IV-D shows that $\frac{\partial \Gamma_1}{\partial \alpha}$ is always positive within $\alpha \in [0,1]$, with a minimum of $0.7241\cdot\Gamma_{\mathrm{LACO}} > 0$ at $\alpha = 0.3074$. Similarly, the partial derivative of Γ_2 with respect to α is

$$\frac{\partial \Gamma_2}{\partial \alpha} = -\frac{2\pi\left(1-\alpha+\pi\sqrt{(1-\alpha)\alpha}\right)\Gamma_{\mathrm{LACO}}}{\sqrt{(1-\alpha)\alpha}\left(2\sqrt{(1-\alpha)\alpha}+\pi\right)^2}, \tag{32}$$

which is always negative within $\alpha \in [0,1]$ having a maximum of $-1.4483\Gamma_{\mathrm{LACO}} < 0$ at $\alpha = 0.6926$. Therefore, upon referring to (29), we have

$$(\mathrm{c}) = \frac{1}{4}\frac{\partial C_{\mathrm{RF}}}{\partial \Gamma_1}\frac{\partial \Gamma_1}{\partial \alpha} \ge 0, \tag{33a}$$

$$\text{and } (\mathrm{d}) = \frac{1}{8}\frac{\partial C_{\mathrm{RF}}}{\partial \Gamma_2}\frac{\partial \Gamma_2}{\partial \alpha} \le 0. \tag{33b}$$

3) Maximum of C_{LACO}: As α approaches 0 from the right hand side, *i.e.* for $\alpha \to 0^+$, the majority of the power would be assigned to layer 2 according to (21), resulting in $P_1 \to 0$ and in turn $\Gamma_1 \to 0$ (linear) or $\Gamma_1 \to -\infty$ (dB). Therefore, (c1) in (29) tends to plus infinity according to Section III-A, while (c2) is a smaller value based on Γ_{LACO}. In this case, we have

$$(\mathrm{c}) = \frac{1}{4}(\mathrm{c1})\cdot(\mathrm{c2}) > -\frac{1}{8}(\mathrm{d1})\cdot(\mathrm{d2}) = -(\mathrm{d}), \tag{34}$$

which yields

$$\left.\frac{\partial C_{\mathrm{LACO}}}{\partial \alpha}\right|_0 > 0. \tag{35}$$

By symmetry, when $\alpha = 1$, part (d) in (29) obeys

$$\left.\frac{\partial C_{\mathrm{LACO}}}{\partial \alpha}\right|_1 < 0. \tag{36}$$

According to Bolzano's theorem [36], for a function which is continuous within an interval, it must be 0 at some point within the interval, if its value is positive at one edge and negative at the other edge. According to (35) and (36), $\frac{\partial C_{\mathrm{LACO}}}{\partial \alpha}$ has opposite signs at the edges of the interval [0,1], hence there must be a zero within the range, yielding:

$$\exists \alpha^* \in [0,1], \text{ s.t. } \left.\frac{\partial C_{\mathrm{LACO}}}{\partial \alpha}\right|_{\alpha^*} = 0. \tag{37}$$

As it will be shown in the next Section, $\frac{\partial C_{\mathrm{LACO}}}{\partial \alpha}$ is actually monotonically decreasing throughout the interval $\alpha \in [0,1]$. Hence, the maximum of C_{LACO} for a particular Γ is obtained at $\alpha = \alpha^*$.

C. Maximum Search

Here, we propose an algorithm for finding the maximum of C_{LACO} for any given Γ, as well as the corresponding optimum α^*.

As seen in Algorithm 1, we commence by entering the modulation order M and the overall channel SNR Γ_{LACO}, as well as the number of Monte-Carlo simulations N used for approximating the capacity and a decision threshold ϵ to determine if the stationary point of C_{LACO} is sufficiently accurate.

Algorithm 1: Power Sharing in Twin-Layer LACO-OFDM.

Input: M, Γ_{LACO}, N, ϵ
Output: α^*, C^*_{LACO}
1: $p := 0, q := 1$;
2: **repeat**
3: $\bar{\alpha} := (p+q)/2$,
4: Calculate $\Gamma_1(\bar{\alpha})$ and $\Gamma_2(\bar{\alpha})$ using (25),
5: Calculate $\frac{\partial C_{\mathrm{LACO}}}{\partial \Gamma_1}|_{\bar{\alpha}}$ and $\frac{\partial C_{\mathrm{LACO}}}{\partial \Gamma_2}|_{\bar{\alpha}}$, by substituting $\Gamma_1(\bar{\alpha})$ and $\Gamma_2(\bar{\alpha})$ into (8), respectively,
6: Calculate $\frac{\partial \Gamma_1}{\partial \alpha}|_{\bar{\alpha}}$ using (31) and $\frac{\partial \Gamma_2}{\partial \alpha}|_{\bar{\alpha}}$ using (32),
7: Calculate $\frac{\partial C_{\mathrm{LACO}}}{\partial \alpha}|_{\bar{\alpha}}$ at α by substituting the above 4 terms into (29);
8: **if** $\frac{\partial C_{\mathrm{LACO}}}{\partial \alpha}|_{\alpha=\bar{\alpha}} > 0$ **then**
9: $p := \bar{\alpha}$,
10: **else**
11: $q := \bar{\alpha}$,
12: **end if**
13: **until** $|\frac{\partial C_{\mathrm{LACO}}}{\partial \alpha}| < \epsilon$;
14: **return** $\alpha^* = \bar{\alpha}$;
15: **return** $C^*_{\mathrm{LACO}} = C_{\mathrm{LACO}}(\alpha^*)$;

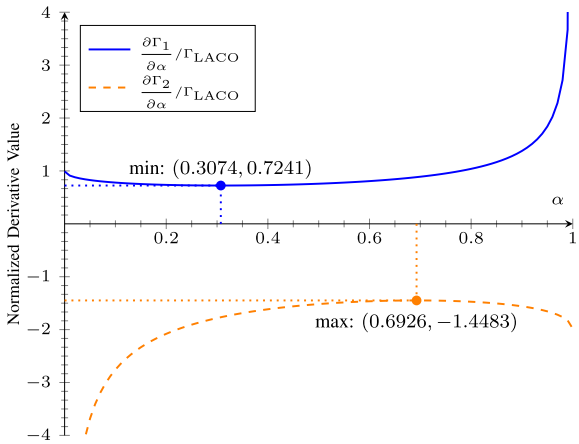

Fig. 7. The normalized derivatives of Γ_1 and Γ_2 in (31) and (32) vs. α.

A binary search philosophy is adopted to find the optimum α^*. A pair of variables, p and q, are employed as the left and right search boundaries, having initial values of 0 and 1, respectively. The testing point of $\bar{\alpha}$ is their average, as in state 3. As discussed before, the optimum value α^* is the stationary point of C_{LACO}. Therefore, a subroutine is provided for calculating the derivative of C_{LACO} at $\bar{\alpha}$. For each $\bar{\alpha}$, states 4–7 of Algorithm 2 calculate its corresponding $\frac{\partial C_{\mathrm{LACO}}}{\partial \alpha}|_{\bar{\alpha}}$ using the equations derived previously in this paper. The binary search part between states 8-12 then proceeds by updating p and q according to the sign of $\frac{\partial C_{\mathrm{LACO}}}{\partial \alpha}|_{\bar{\alpha}}$, which in turn updates $\bar{\alpha}$ in the next optimization iteration. This process will gradually shrink the search window, eventually finding the optimum α^* within an accuracy of ϵ.

D. Numerical Results

Fig. 7 plots the partial derivatives of Γ_1 and Γ_2 with respect to α based on (31) and (32), whose derivatives have been normalized by Γ_{LACO}. It is clearly shown that $\frac{\partial \Gamma_1}{\partial \alpha}$ is always positive, while $\frac{\partial \Gamma_2}{\partial \alpha}$ is always negative, in line with (35) and (36). Fig. 8 shows the channel capacity of twin-layer LACO-OFDM using 16QAM both vs. the overall SNR and vs. the power sharing factor α. Focusing our attention on the SNR axis, it is clear that the channel capacity converges to 1.5 bits/symbol upon increasing the SNR. This agrees with (26), because we have $\lim_{\Gamma\to\infty} C_{\mathrm{RF}(\Gamma)} = 4$ for 16QAM. Similar trends can be found for all SNR values, namely that as α is increased from 0 to 1, the corresponding capacity first significantly increases and then decreases, albeit its maximum is not very pronounced. A more clear view is provided in Fig. 9, where both the capacity as well as its derivative are plotted against α at SNR $= 12$ dB. The channel capacity increases up to the power sharing factor of $\alpha = 0.6841$, reaching a maximum of 1.3498 bits/symbol, before falling again. The corresponding derivative is monotonically decreasing and has a zero-crossing at $\alpha = 0.6841$, which verifies Algorithm 1.

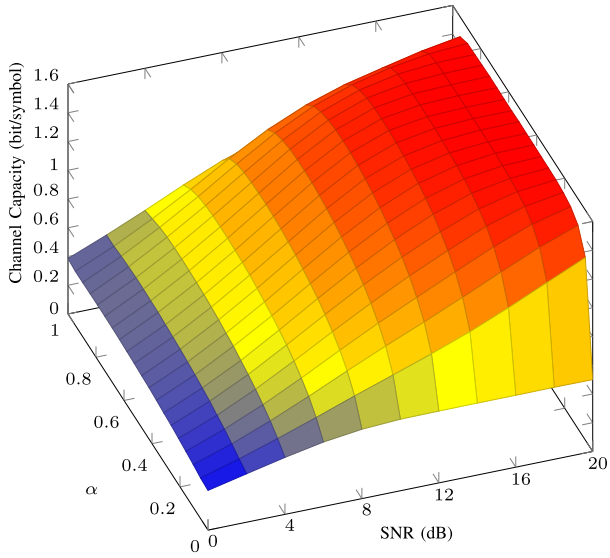

Fig. 8. α and SNR versus channel capacity of a twin-layer LACO-OFDM using 16QAM.

Meanwhile, Fig. 9 also indicates that the conventional power sharing strategy of $\frac{P_1}{P_2} = 2$, corresponding to $\alpha = \frac{2}{3} \approx 0.6666$, yields a lower capacity. Up to this point, the derivative still remains positive, hence the capacity still increases with α. This trend will be further discussed in Section VI. Moreover, the optimum channel capacity versus SNR for twin-layer LACO-OFDM associated with different modulation schemes is portrayed in Fig. 10.

V. Capacity Maximization for Multi-Layer LACO-OFDM

In this section, we explore the capacity maximization problem of 3-layer LACO-OFDM systems, before generalizing it to multi-layer LACO-OFDM systems. In subsections A to C, the variables P_{LACO}, Γ_{LACO} and C_{LACO} represent the corresponding metrics of a 3-layer LACO-OFDM system, while in subsection D, they are for L-layer LACO-OFDM systems.

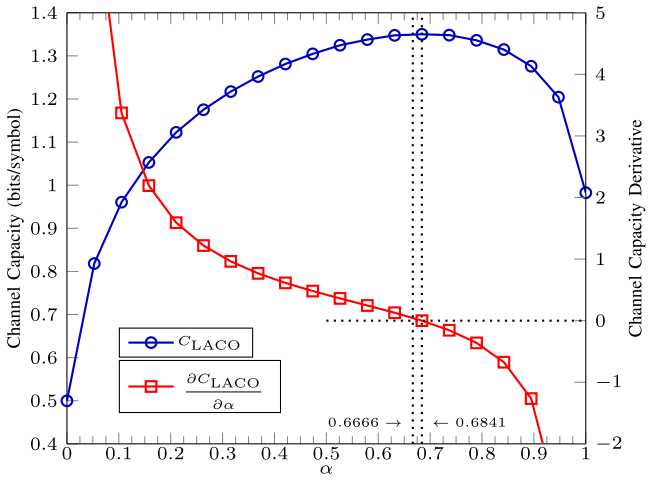

Fig. 9. Channel capacity and its derivative for twin-layer LACO-OFDM using 16QAM at SNR = 12 dB vs. the power sharing factor α.

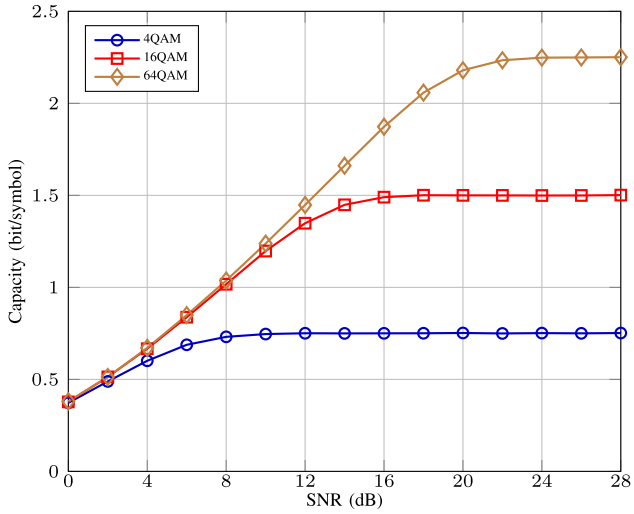

Fig. 10. Optimized capacity of twin-layer LACO-OFDM using Algorithm 1 vs. the SNR.

A. Capacity of 3-Layer LACO-OFDM

For 3-layer LACO-OFDM systems, the relationships between the power of the three layers can be reflected by introducing a pair of power sharing factors: α_1 and α_2:

$$\frac{P_1}{P_2} = \frac{\alpha_1}{1-\alpha_1} \text{ and } \frac{P_1}{P_3} = \frac{\alpha_2}{1-\alpha_2}, \tag{38}$$

where $0 \le \alpha_1 \le 1$ and $0 \le \alpha_2 \le 1$.

Based on (15), the overall power of the 3-layer LACO-OFDM system can now be expressed purely in terms of P_1, as seen in (39) shown at bottom of this page. Therefore, with the additional help of (38), the SNR of each layer can be expressed as

$$\Gamma_1 = \frac{P_1}{N_0/2} = \frac{\alpha_1\alpha_2 \cdot \Gamma_{\mathrm{LACO}}}{\mathrm{P}^\star}, \tag{40a}$$

$$\Gamma_2 = \frac{2P_2}{N_0/2} = \frac{2(1-\alpha_1)\alpha_2 \cdot \Gamma_{\mathrm{LACO}}}{\mathrm{P}^\star}, \tag{40b}$$

$$\Gamma_3 = \frac{4P_3}{N_0/2} = \frac{4\alpha_1(1-\alpha_2) \cdot \Gamma_{\mathrm{LACO}}}{\mathrm{P}^\star}, \tag{40c}$$

where $\mathrm{P}^\star$ was defined in (39), which is a function of both α_1 and α_2. The overall DCMC capacity of 3-layer LACO-OFDM can then be expressed as the sum of the 3 layers' capacities:

$$\begin{aligned} C_{\mathrm{LACO}} &= C_1(\Gamma_1) + C_2(\Gamma_2) + C_3(\Gamma_3) \\ &= \frac{C_{\mathrm{RF}}(\Gamma_1)}{4} + \frac{C_{\mathrm{RF}}(\Gamma_2)}{8} + \frac{C_{\mathrm{RF}}(\Gamma_3)}{16}. \end{aligned} \tag{41}$$

Apparently, for any given total SNR (Γ_{LACO}), C_{LACO} depends[3] on both α_1 and α_2. Bearing this in mind, let us now study the associated capacity maximization problem.

B. Maximization of 3-Layer LACO-OFDM Capacity

The extreme values of the dual-variable function C_{LACO} will only occur at points, where its gradient equals zero. Therefore, the partial derivatives of C_{LACO} with respect to α_1 and α_2 are expressed as:

$$\begin{aligned} &\frac{\partial C_{\mathrm{LACO}}}{\partial \alpha_1} \\ &= \frac{1}{4}\frac{\partial C_{\mathrm{RF}}}{\partial \Gamma_1}\frac{\partial \Gamma_1}{\partial \alpha_1} + \frac{1}{8}\frac{\partial C_{\mathrm{RF}}}{\partial \Gamma_2}\frac{\partial \Gamma_2}{\partial \alpha_1} + \frac{1}{16}\frac{\partial C_{\mathrm{RF}}}{\partial \Gamma_3}\frac{\partial \Gamma_3}{\partial \alpha_1}, \end{aligned} \tag{42a}$$

[3] At the moment, all other variables, such as M and N, are treated as constants.

$$\begin{aligned} P_{\mathrm{LACO}} &= P_1 + P_2 + P_3 + \frac{2}{\pi}\left(\sqrt{P_1P_2} + \sqrt{P_1P_3} + \sqrt{P_2P_3}\right) \\ &= P_1 + \frac{1-\alpha_1}{\alpha_1}P_1 + \frac{1-\alpha_2}{\alpha_2}P_1 + \frac{2}{\pi}\left(\sqrt{P_1 \cdot \frac{1-\alpha_1}{\alpha_1}P_1} + \sqrt{P_1 \cdot \frac{1-\alpha_2}{\alpha_2}P_1} + \sqrt{\frac{1-\alpha_1}{\alpha_1}P_1 \cdot \frac{1-\alpha_2}{\alpha_2}P_1}\right) \\ &= P_1\left[1 + \frac{1-\alpha_1}{\alpha_1} + \frac{1-\alpha_2}{\alpha_2} + \frac{2}{\pi}\left(\sqrt{\frac{1-\alpha_1}{\alpha_1}} + \sqrt{\frac{1-\alpha_2}{\alpha_2}} + \sqrt{\frac{(1-\alpha_1)(1-\alpha_2)}{\alpha_1\alpha_2}}\right)\right] \\ &= \frac{P_1}{\alpha_1\alpha_2} \cdot \underbrace{\left[\alpha_1 + \alpha_2 - \alpha_1\alpha_2 + \frac{2}{\pi}\left(\alpha_2\sqrt{\alpha_1(1-\alpha_1)} + \alpha_1\sqrt{\alpha_2(1-\alpha_2)} + \sqrt{\alpha_1\alpha_2(1-\alpha_1)(1-\alpha_2)}\right)\right]}_{\mathrm{P}^\star} \end{aligned} \tag{39}$$

$$\frac{\partial C_{\mathrm{LACO}}}{\partial \alpha_2} = \frac{1}{4}\frac{\partial C_{\mathrm{RF}}}{\partial \Gamma_1}\frac{\partial \Gamma_1}{\partial \alpha_2} + \frac{1}{8}\frac{\partial C_{\mathrm{RF}}}{\partial \Gamma_2}\frac{\partial \Gamma_2}{\partial \alpha_2} + \frac{1}{16}\frac{\partial C_{\mathrm{RF}}}{\partial \Gamma_3}\frac{\partial \Gamma_3}{\partial \alpha_2}. \quad (42b)$$

The characteristics of C_{LACO} are similar to those of its twin-layer counterpart shown in Section IV-B, which is monotonically increasing and then decreasing within [0,1] for both α_1 and α_2. The optimum point (α_1^*, α_2^*) can be found by solving

$$\mathrm{diag}\{\nabla C_{\mathrm{LACO}}(\alpha_1, \alpha_2)\} = \mathbf{0}. \quad (43)$$

Note that

$$\frac{\partial \Gamma_1}{\partial \alpha_1} = \frac{\Gamma_{\mathrm{LACO}}}{(\mathrm{P}^\star)^2}\left(\alpha_2 \mathrm{P}^\star - \alpha_1\alpha_2\frac{\partial \mathrm{P}^\star}{\partial \alpha_1}\right), \quad (44a)$$

$$\frac{\partial \Gamma_2}{\partial \alpha_1} = \frac{\Gamma_{\mathrm{LACO}}}{(\mathrm{P}^\star)^2}\left(-2\alpha_2 \mathrm{P}^\star - \alpha_1\alpha_2\frac{\partial \mathrm{P}^\star}{\partial \alpha_1}\right), \quad (44b)$$

$$\frac{\partial \Gamma_3}{\partial \alpha_1} = \frac{\Gamma_{\mathrm{LACO}}}{(\mathrm{P}^\star)^2}\left(4(1-\alpha_2)\mathrm{P}^\star - \alpha_1\alpha_2\frac{\partial \mathrm{P}^\star}{\partial \alpha_1}\right), \quad (44c)$$

where

$$\frac{\partial \mathrm{P}^\star}{\partial \alpha_1} = 1 - \alpha_2 + \frac{2}{\pi}\sqrt{\alpha_2(1-\alpha_2)} + \frac{(1-2\alpha_1)\left(\alpha_2 + \sqrt{\alpha_2(1-\alpha_2)}\right)}{\pi\sqrt{\alpha_2(1-\alpha_2)}}; \quad (44d)$$

and

$$\frac{\partial \Gamma_1}{\partial \alpha_2} = \frac{\Gamma_{\mathrm{LACO}}}{(\mathrm{P}^\star)^2}\left(\alpha_1 \mathrm{P}^\star - \alpha_1\alpha_2\frac{\partial \mathrm{P}^\star}{\partial \alpha_2}\right), \quad (44e)$$

$$\frac{\partial \Gamma_2}{\partial \alpha_2} = \frac{\Gamma_{\mathrm{LACO}}}{(\mathrm{P}^\star)^2}\left(2(1-\alpha_1)\mathrm{P}^\star - \alpha_1\alpha_2\frac{\partial \mathrm{P}^\star}{\partial \alpha_2}\right), \quad (44f)$$

$$\frac{\partial \Gamma_3}{\partial \alpha_2} = \frac{\Gamma_{\mathrm{LACO}}}{(\mathrm{P}^\star)^2}\left(-4\alpha_1 \mathrm{P}^\star - \alpha_1\alpha_2\frac{\partial \mathrm{P}^\star}{\partial \alpha_2}\right), \quad (44g)$$

where

$$\frac{\partial \mathrm{P}^\star}{\partial \alpha_2} = 1 - \alpha_1 + \frac{2}{\pi}\sqrt{\alpha_1(1-\alpha_1)} + \frac{(1-2\alpha_2)\left(\alpha_1 + \sqrt{\alpha_1(1-\alpha_1)}\right)}{\pi\sqrt{\alpha_2(1-\alpha_2)}}. \quad (44h)$$

Since α_1 appears in the expressions of (44e–44h) and α_2 in (44a–44d), a nested algorithm is required for solving (43).

As shown in Algorithm 2, the search is conducted in the twinned directions: of α_1 and α_2, respectively. The inner loop is detailed in Algorithm 3, which takes a given value of $\bar{\alpha}_1$ and substitutes it into (42b), followed by finding the corresponding α_2 coordinate, where the zero-crossing occurs, using similar methods to those in Algorithm 1.

The outer loop of Algorithm 2 then takes the returned value $\bar{\alpha}_2$ to determine whether a zero-crossing has also be found for (42a). If not, $\bar{\alpha}_1$ will be updated in a binary-search manner and forwarded to Algorithm 3 for the corresponding new $\bar{\alpha}_2$. The process continues by checking and updating $\bar{\alpha}_1$ and $\bar{\alpha}_2$, until a zero-crossing occurs in both directions, thus reaching the stationary point.

Algorithm 2: Power Sharing in 3-Layer LACO-OFDM.

Input: M, Γ_{LACO}, N, ϵ
Output: α_1^*, α_2^*, C_{LACO}^*

$p_1 := 0$, $q_1 := 1$
repeat
  $\bar{\alpha}_1 := (p_1 + q_1)/2$,
  Find $\bar{\alpha}_2$ under current $\bar{\alpha}_1$ using Algorithm 3;
  Calculate $\Gamma_l(\bar{\alpha}_1, \bar{\alpha}_2)$ for $l = 1, 2, 3$ using (40),
  Calculate $\frac{\partial C_{\mathrm{LACO}}}{\partial \Gamma_l}|_{(\bar{\alpha}_1, \bar{\alpha}_2)}$ for $l = 1, 2, 3$ using (32),
  Calculate $\frac{\partial \Gamma_l}{\partial \alpha_1}|_{(\bar{\alpha}_1, \bar{\alpha}_2)}$ for $l = 1, 2, 3$ using (44),
  Calculate $\frac{\partial C_{\mathrm{LACO}}}{\partial \alpha_1}|_{(\bar{\alpha}_1, \bar{\alpha}_2)}$ by substituting the above 6 terms into (42a);
  if $\frac{\partial C_{\mathrm{LACO}}}{\partial \alpha_1}|_{(\bar{\alpha}_1, \bar{\alpha}_2)} > 0$ **then**
    $p_1 := \bar{\alpha}_1$,
  else
    $q_1 := \bar{\alpha}_1$,
  end if
until $\frac{\partial C_{\mathrm{LACO}}}{\partial \alpha_1}|_{(\bar{\alpha}_1, \bar{\alpha}_2)} < \epsilon$ at (α_1, α_2);
return $\alpha_1^* = \bar{\alpha}_1$, $\alpha_2^* = \bar{\alpha}_2$;
return $C_{\mathrm{LACO}}^* = C_{\mathrm{LACO}}(\alpha_1^*, \alpha_2^*)$;

Algorithm 3: Zero Crossing Finder for Eq. (42b).

Input: M, Γ_{LACO}, N, ϵ, $\bar{\alpha}_1$
Output: $\bar{\alpha}_2$

$p_2 := 0$, $q_2 := 1$;
repeat
  $\bar{\bar{\alpha}}_2 := (p_2 + q_2)/2$,
  Calculate $\Gamma_l(\bar{\alpha}_1, \bar{\bar{\alpha}}_2)$ for $l = 1, 2, 3$ using (40),
  Calculate $\frac{\partial C_{\mathrm{LACO}}}{\partial \Gamma_l}$ at $\Gamma_l(\bar{\alpha}_1, \bar{\bar{\alpha}}_2)$ for $l = 1, 2, 3$ using (32),
  Calculate $\frac{\partial \Gamma_l}{\partial \alpha_2}|_{(\bar{\alpha}_1, \bar{\bar{\alpha}}_2)}$ for $l = 1, 2, 3$ using (44),
  Calculate $\frac{\partial C_{\mathrm{LACO}}}{\partial \alpha_2}|_{(\bar{\alpha}_1, \bar{\bar{\alpha}}_2)}$ by substituting the above 6 terms into (42b);
  if $\frac{\partial C_{\mathrm{LACO}}}{\partial \alpha_2}|_{(\bar{\alpha}_1, \bar{\bar{\alpha}}_2)} > 0$ **then**
    $p_2 := \bar{\bar{\alpha}}_2$,
  else
    $q_2 := \bar{\bar{\alpha}}_2$,
  end if
until $\frac{\partial C_{\mathrm{LACO}}}{\partial \alpha_2}|_{(\bar{\alpha}_1, \bar{\bar{\alpha}}_2)} < \epsilon$;
return $\bar{\alpha}_2 = \bar{\bar{\alpha}}_2$;

C. Numerical Results

In Fig. 11, we portray the channel capacity of a 3-layer LACO-OFDM system vs. its power sharing factors α_1 and α_2, using 16QAM at an SNR of 12 dB. Observe that the capacity first increases and then decreases with respect to both α_1 and α_2, resulting in a global peak in the middle.

To elaborate a little further, in Fig. 12 we provide cross-sectional views of the capacity by slicing the 3D surface of

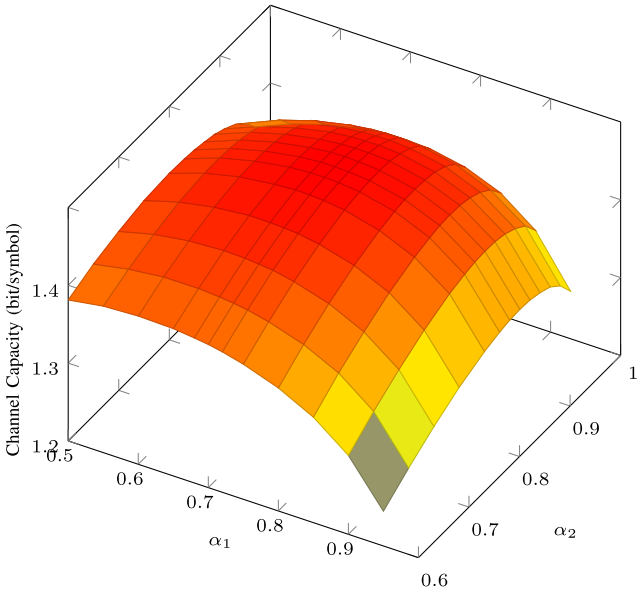

Fig. 11. Channel capacity of 3-Layer LACO-OFDM using 16QAM at SNR = 12 dB vs. α_1 and α_2.

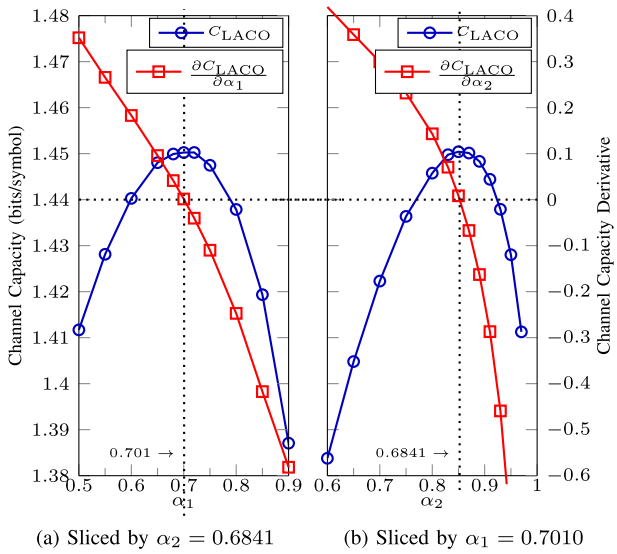

(a) Sliced by $\alpha_2 = 0.6841$ (b) Sliced by $\alpha_1 = 0.7010$

Fig. 12. Channel capacity of 3-layer LACO-OFDM extracted from Fig. 11 and its derivatives.

Fig. 11 along α_1 and α_2, respectively. The derivatives with respect to the corresponding variables are also depicted in the same figure. In Fig. 12(a), the capacity peak can be found at the zero crossing of its derivative, namely at $\alpha_1 = 0.701$. Fig. 12(b) is then sliced by the vertical plane at $\alpha_1 = 0.701$, leading to the same capacity peak at $\alpha_2 = 0.6841$, which in turn decides where to slice it for generating Fig. 12(a). Since the capacity derivatives are zero in both directions at $(\alpha_1, \alpha_2) = (0.701, 0.6841)$, the peak constitutes a global capacity maximum.

To provide further insights, Fig. 13 depicts the optimum channel capacity versus SNR for 3-layer LACO-OFDM in conjunction with different modulation schemes. More detailed discussions regarding the capacity improvement will be included in Section VI-A.

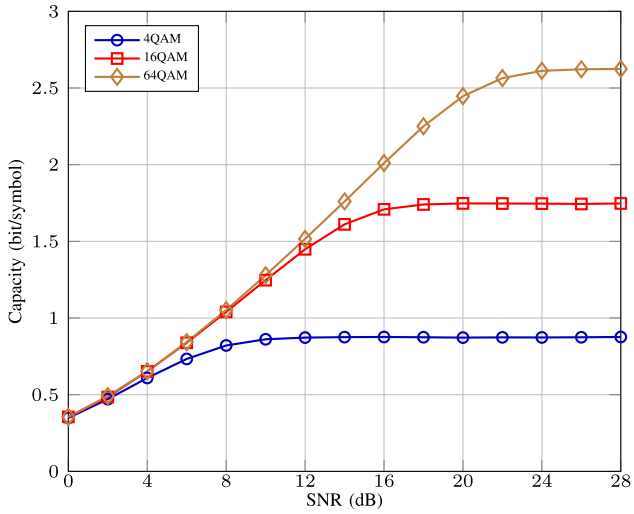

Fig. 13. Optimized DCMC capacity of 3-Layer LACO-OFDM vs. SNR using the proposed algorithm.

D. Generalization of the Algorithm

Let us now continue by summarizing the optimum power sharing of 3-layer LACO-OFDM systems and by generalizing it for L-layer LACO-OFDM.

1) Let us establish the power sharing factors using $\boldsymbol{\alpha} = [\alpha_1, \ldots, \alpha_l, \ldots, \alpha_{L-1}]$, and
$$\frac{P_1}{P_l} = \frac{\alpha_{l-1}}{1-\alpha_{l-1}}, 0 \leq \alpha_{l-1} \leq 1. \tag{45}$$
2) Let us then express the SNRs of each layer Γ_l in terms of the total SNR Γ_{LACO} and $\boldsymbol{\alpha}$, using (15) and (16).
3) Obtain the total capacity formula C_{LACO} using (19), and differentiate it with respect to every element of $\boldsymbol{\alpha}$.
4) Using an $(L-1)$-stage nested loop in the power-sharing algorithm to find the maximum of C_{LACO}, we carry out the following steps:
   a) Fix the values of $\alpha_1, \ldots \alpha_{L-2}$ and substitute them into $\frac{\partial C_{\mathrm{LACO}}}{\partial \alpha_{L-1}} = 0$. Find the root α_{L-1} using binary search within [0,1] and return to its upper loop.
   b) Sweep the value of α_{L-2} across its legitimate range and calculate the corresponding α_{L-1} each time, until $\frac{\partial C_{\mathrm{LACO}}}{\partial \alpha_{L-2}} = 0$ is reached. Forward α_{L-1} and α_{L-2} to the upper loop.
   c) Repeat this procedure until the top stage of the loop is reached and find the values of all elements in $\boldsymbol{\alpha}$ so that we have $\mathrm{diag}\{\nabla C_{\mathrm{LACO}}\} = \mathbf{0}$.

VI. Discussions

A. Comparison to Conventional Power Sharing Strategy

In previous contributions on LACO-OFDM [15], [23], [25], the "equal power per bit" strategy has been employed, where the same amount of power is assigned to all information bits in the system, regardless of their location in the layers. Explicitly, if the same modulation order is applied for all layers, each layer should have twice the energy of its directly-following layer, because

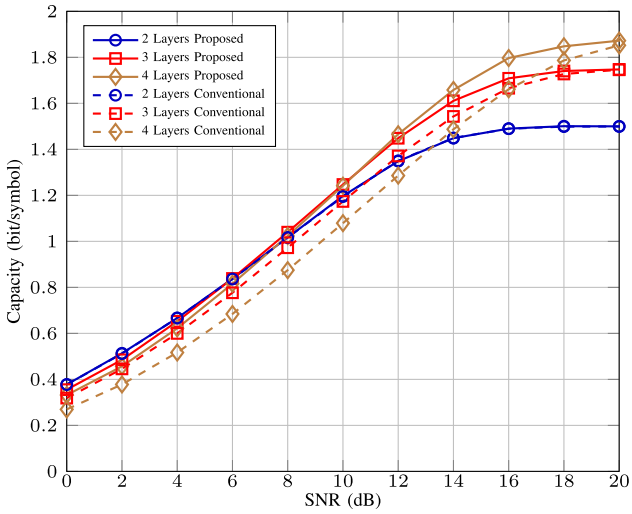

Fig. 14. Capacity comparison for LACO-OFDM schemes using conventional and proposed power sharing algorithms. 16QAM modulation is used for all simulations.

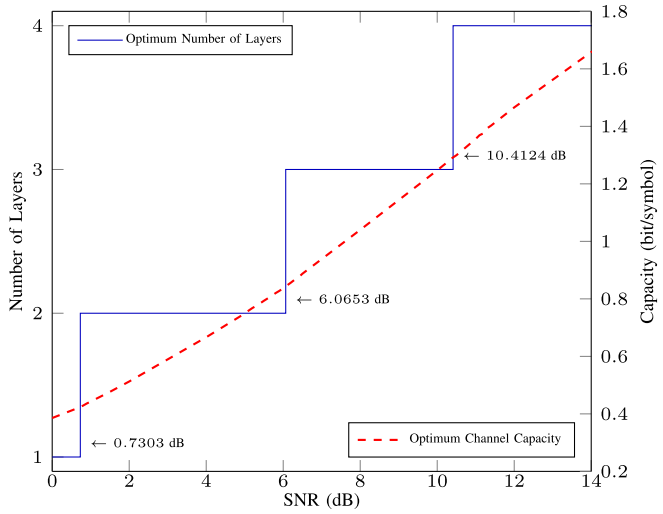

Fig. 15. Adaptive layer number selection for maximum capacity in LACO-OFDM based on the SNR.

the former transmits twice the amount of information bits than the latter. This leads to a fixed $\boldsymbol{\alpha} = \{\alpha_1, \alpha_2, \ldots \alpha_{L-1}\}$ vector, regardless of the channel SNR. According to (45), we have

$$\alpha_l = \frac{P_1}{P_1 + P_{l+1}} = \frac{2^l P_{l+1}}{2^l P_{l+1} + P_{l+1}} = \frac{1}{1 + 2^{-l}}. \tag{46}$$

In Fig. 14, we compare the capacity improvement attained by using the Algorithm proposed. Observe that the "equal power per bit" strategy is outperformed by the proposed one.

Specifically, at SNR $= 12$ dB, a beneficial capacity improvement of about 0.18 bits/symbol can be attained by 4-layer LACO-OFDM using 16QAM. From a different prospective, this can also be equivalently expressed as a 1.8 dB SNR gain, because the conventional strategy reaches the same capacity at a 1.8 dB higher SNR. By contrast, the difference for a twin-layer system remains negligible.

B. Adapting the Number of Layers

It may also be observed from Fig. 14 that the capacity curves do cross each other, before saturating for SNR ≥ 20 dB. LACO-OFDM schemes having more layers have lower capacity in the low-SNR region before crossing all other curves. In the spirit of achieving the maximum capacity, we propose to adapt the number of layers based on the overall SNR.

In Fig. 15, an example is provided for 16QAM LACO-OFDM, where the number of layers ranges from 1 to 4, with 1 representing ACO-OFDM instead of LACO-OFDM. In this case, when the SNR is lower than 0.7303 dB, using the second layer is in fact detrimental, because the power has to be shared between two layers. Beyond that point, utilizing LACO-OFDM shows capacity benefits. The handover between 2- and 3-layer LACO-OFDM occurs at SNR $= 6.0653$ dB, where they have equal capacity, and for 3- and 4-layer it is at SNR $= 10.4124$ dB.

The transmitter would require the channel SNR to be fed back from the receiver to the transmitter and determine the number of layers to use, based on which interval of Fig. 15 the SNR lies in. It will then find the optimum power sharing strategy using our proposed algorithm, which can be represented by a look-up table.

VII. Conclusion

The DCMC capacity of LACO-OFDM has been derived for a given number of layers relying on our power sharing strategy. The capacity formula was then used as our objective function to maximize the capacity by tuning the power sharing factors and the number of layers as well. Specific algorithms have been proposed for solving optimization problem with the help of partial derivatives. Recursive algorithms were designed for our systems having more than 2 layers. The numerical results show an up to 0.18 bits/symbol increase of the capacity upon adopting the proposed power sharing strategy instead of the conventional one for 4-layer LACO-OFDM. Finally, an adaptive scheme was conceived for maximizing the DCMC capacity of LACO-OFDM relying on adapting the number of layers depending on the SNR encountered.

Acknowledgment

The authors would like to thank the anonymous reviewers for their precious time, valuable comments and inspirational suggestions for improving the paper.

References

[1] S. Dimitrov and H. Haas, *Principles of LED Light Communications: Towards Networked Li-Fi*. Cambridge, U.K.: Cambridge Univ. Press, 2015.
[2] Z. Wang, Q. Wang, W. Huang, and Z. Xu, *Visible Light Communications: Modulation and Signal Processing*. Hoboken, NJ, USA: Wiley, 2018.
[3] P. H. Pathak, X. Feng, P. Hu, and M. Mohapatra, "Visible light communication networking and sensing: A survey potential and challenges," *IEEE Commun. Survey Tuts*, vol. 17, no. 4, pp. 2047–2077, Oct.–Dec. 2015.
[4] J. M. Kahn and J. R. Barry, "Wireless infrared communications," *Proc. IEEE*, vol. 85, no. 2, pp. 265–198, Feb. 1997.

[5] L. Hanzo, M. Münster, B. J. Choi, and T. Keller, *OFDM and MC-CDMA for Broadband Multi-User Communications, WLANs and Broadcasting*. Chichester, U.K.: Wiley, 2003.
[6] L. Hanzo, T. H. Liew, B. L. Yeap, R. Y. S. Tee, and S. X. Ng, *Turbo Coding, Turbo Equalisation and Space-Time Coding: EXIT-Chart-Aided Near-Capacity Designs for Wireless Channels*. Chichester, U.K.: Wiley, 2011.
[7] J. Armstrong, "OFDM for optical communications," *J. Lightw. Technol.*, vol. 27, no. 3, pp. 189–204, Feb. 2009.
[8] J. B. Carruthers and J. M. Kahn, "Multiple-subcarrier modulation for nondirected wireless infrared communication," *IEEE J. Sel. Areas Commun.*, vol. 14, no. 3, pp. 538–546, Apr. 1996.
[9] J. Armstrong and A. Lowery, "Power efficient optical OFDM," *Electron. Lett.*, vol. 42, pp. 370–372, Mar. 2006.
[10] S. D. Dissanayake and J. Armstrong, "Comparison of ACO-OFDM, DCO-OFDM and ADO-OFDM in IM/DD systems," *J. Lightw. Technol.*, vol. 31, no. 7, pp. 1063–1072, Apr. 2013.
[11] S. Lu, I. A. Hemadeh, M. El-Hajjar, and L. Hanzo, "Compressed-sensing-aided space-time frequency index modulation," *IEEE Trans. Veh. Technol.*, vol. 67, no. 7, pp. 6259–6271, Jul. 2018.
[12] S. Lu, M. El-Hajjar, and L. Hanzo, "Two-dimensional index modulation for the large-scale multi-user MIMO uplink," *IEEE Trans. Veh. Technol.*, vol. 68, no. 8, pp. 7904–7918, Aug. 2019.
[13] S. D. Dissanayake, K. Panta, and J. Armstrong, "A novel technique to simultaneously transmit ACO-OFDM and DCO-OFDM in IM/DD systems," in *Proc. IEEE Glob. Commun. Conf. Workshop*, Houston, TX, USA, Dec. 2011, pp. 782–786.
[14] B. Ranjha and M. Kavehrad, "Hybrid asymmetrically clipped OFDM-based IM/DD optical wireless system," *IEEE/OSA J. Opt. Commun. Netw.*, vol. 6, no. 4, pp. 387–396, Apr. 2014.
[15] Q. Wang, C. Qian, X. Guo, Z. Wang, D. G. Cunningham, and I. H. White, "Layered ACO-OFDM for intensity-modulated direct-detection optical wireless transmission," *Opt. Express*, vol. 23, pp. 12382–12393, May 2015.
[16] R. Bai, Q. Wang, and Z. Wang, "Asymmetrically clipped absolute value optical OFDM for intensity-modulated direct-detection systems," *J. Lightw. Technol.*, vol. 35, no. 17, pp. 3680–3691, Sep. 2017.
[17] H. Elgala and T. D. C. Little, "SEE-OFDM: Spectral and energy efficient OFDM for optical IM/DD systems," in *Proc. IEEE 25th Annu. Int. Symp. Pers. Indoor Mobile Radio Commun.*, Washington, DC, USA, Sep. 2014, pp. 851–855.
[18] E. Lam, S. K. Wilson, H. Elgala, and T. D. C. Little, "Spectrally and energy efficient OFDM (SEE-OFDM) for intensity modulated optical wireless systems," 2015, *arXiv:1510.08172*.
[19] M. S. Islim, D. Tsonev, and H. Haas, "On the superposition modulation for OFDM-based optical wireless communication," in *Proc. IEEE Global Conf. Signal Inf. Process.*, Orlando, FL, USA, Dec. 2015, pp. 1022–1026.
[20] A. J. Lowery, "Enhanced asymmetrically clipped optical ODFM for high spectral efficiency and sensitivity," in *Proc. Opt. Fiber Commun. Conf. Exhib.*, Anaheim, CA, USA, Mar. 2016, pp. 1–3.
[21] D. Tsonev and H. Haas, "Avoiding spectral efficiency loss in unipolar OFDM for optical wireless communication," in *Proc. IEEE Int. Conf. Commun.*, Sydney, NSW, Australia, Jun. 2014, pp. 3336–3341.
[22] D. Tsonev, S. Videv, and H. Haas, "Unlocking spectral efficiency in intensity modulation and direct detection systems," *IEEE J. Sel. Areas Commun.*, vol. 33, no. 9, pp. 1758–1770, Sep. 2015.
[23] X. Zhang, Q. Wang, R. Zhang, S. Chen, and L. Hanzo, "Performance analysis of layered ACO-OFDM," *IEEE Access*, vol. 5, pp. 18366–18381, 2017.
[24] X. Zhang, Z. Babar, R. Zhang, S. Chen, and L. Hanzo, "Multi-class coded layered asymmetrically clipped optical OFDM," *IEEE Trans. Commun.*, vol. 67, no. 1, pp. 578–589, Jan. 2019.
[25] Z. Babar *et al.*, "Near-capacity multilayered code design for LACO-OFDM-aided optical wireless systems," *IEEE Trans. Veh. Technol.*, vol. 68, no. 4, pp. 4051–4054, Apr. 2019.
[26] X. Li, J. Vucic, V. Jungnickel, and J. Armstrong, "On the capacity of intensity-modulated direct-detection systems and the information rate of ACO-OFDM for indoor optical wireless applications," *IEEE Trans. Commun.*, vol. 60, no. 3, pp. 799–809, Mar. 2012.
[27] J. Zhou and W. Zhang, "A comparative study of unipolar OFDM schemes in Gaussian optical intensity channel," *IEEE Trans. Commun.*, vol. 66, no. 4, pp. 1549–1564, Apr. 2018.
[28] Y. Sun, F. Yang, and J. Gao, "Comparison of hybrid optical modulation schemes for visible light communication," *IEEE Photon. J.*, vol. 9, no. 3, pp. 1–13, Jun. 2017.
[29] Y. Sun, F. Yang, and J. Gao, "Near-optimal power allocation and layer assignment for LACO-OFDM in visible light communication," in *Proc. IEEE Global Commun. Conf.*, Singapore, Dec. 2017, pp. 1–6.
[30] C. E. Shannon, "A mathematical theory of communication," *Bell Syst. Tech. J.*, vol. 27, pp. 379–423, Jul. 1948.
[31] R. Mesleh, H. Elgala, and H. Haas, "Performance analysis of indoor OFDM optical wireless communication systems," in *Proc. IEEE Wireless Commun. Netw. Conf.*, Paris, France, Apr. 2012, pp. 1005–1010.
[32] J. Armstrong and B. J. C. Schmidt, "Comparison of asymmetrically clipped optical OFDM and DC-biased optical OFDM in AWGN," *IEEE Commun. Lett.*, vol. 12, no. 5, pp. 343–345, May 2008.
[33] J. B. Carruthers and J. M. Kahn, "Modeling of nodirected wireless infrared channels," *IEEE Trans. Commun.*, vol. 45, no. 10, pp. 1260–1268, Oct. 1997.
[34] Z. Babar, S. X. Ng, and L. Hanzo, "Near-capacity code design for entanglement-assisted classical communication over quantum depolarizing channels," *IEEE Trans. Commun.*, vol. 61, no. 12, pp. 4801–4807, Dec. 2013.
[35] W. Ryan and S. Lin, *Channel Codes: Classical and Modern*. New York, NY, USA: Cambridge Univ. Press, 2009.
[36] R. A. Adams and C. Essex, *Calculus: A Complete Course*, 7 ed. Toronto, ON, Canada: Pearson, 2010.

Xiaoyu Zhang (Student Member, IEEE) received the B.Eng. degree in electronic information engineering from the University of Electronic Science and Technology of China, Chengdu, China, in 2014 and the M.Sc. and Ph.D. degrees from the University of Southampton, Southampton, U.K., in 2015 and 2020, respectively. He is currently an Adjunct Research Associate with the Next Generation Wireless Group, University of Southampton. His research interests lie in the areas of wireless and fiber optical communications.

Sheng Chen (Fellow, IEEE) received the B.Eng. degree in control engineering from the East China Petroleum Institute, Dongying, China, in 1982, the Ph.D. degree in control engineering from the City University of London, London, U.K., in 1986, and the higher doctoral degree (D.Sc.) from the University of Southampton, Southampton, U.K., in 2005. He held research and academic appointments with the University of Sheffield, the University of Edinburgh, and the University of Portsmouth, U.K., from 1986 to 1999. Since 1999, he has been with the Department of Electronics and Computer Science, University of Southampton, where he is currently a Professor of Intelligent Systems and Signal Processing. His research interests include adaptive signal processing, wireless communications, modeling and identification of nonlinear systems, neural network and machine learning, intelligent control system design, evolutionary computation methods, and optimization. He has authored more than 550 research papers. He is a Fellow of the United Kingdom Royal Academy of Engineering, a Fellow of IET, and a Distinguished Adjunct Professor with King Abdulaziz University, Jeddah, Saudi Arabia. He was an ISI Highly Cited Researcher in engineering in 2004.

Lajos Hanzo (Fellow, IEEE) received the master's and doctorate degrees from the Technical University (TU) of Budapest, Budapest, Hungary, in 1976 and 1983, respectively, the Doctor of Sciences (D.Sc.) degree from the University of Southampton, Southampton, U.K., in 2004, and the Honorary Doctorate degree from the TU of Budapest, Budapest, Hungary, in 2009 and The University of Edinburgh, Edinburgh, U.K., in 2015. He is a Foreign Member of the Hungarian Academy of Sciences and a former Editor-in-Chief of the IEEE Press. He has served several terms as a Governor of both IEEE ComSoc and of VTS. He has authored or coauthored more than 1900 contributions at IEEE Xplore, 19 Wiley-IEEE Press books, and has helped the fast-track career of 123 Ph.D. students. More thann 40 of them are Professors at various stages of their careers in academia and many of them are leading scientists in the wireless industry. He is a Fellow of the Royal Academy of Engineering F(REng), the IET, and EURASIP.